Multiregion Level-Set Partitioning of Synthetic Aperture Radar Images

Ismail Ben Ayed, *Student Member*, *IEEE*, Amar Mitiche, *Member*, *IEEE*, and Ziad Belhadj, *Member*, *IEEE*

Abstract—The purpose of this study is to investigate Synthetic Aperture Radar (SAR) image segmentation into a given but arbitrary number of gamma homogeneous regions via active contours and level sets. The segmentation of SAR images is a difficult problem due to the presence of speckle which can be modeled as strong, multiplicative noise. The proposed algorithm consists of evolving simple closed planar curves within an explicit correspondence between the interiors of curves and regions of segmentation to minimize a criterion containing a term of conformity of data to a speckle model of noise and a term of regularization. Results are shown on both synthetic and real images.

Index Terms—Image segmentation, active contours, level sets, statistical modeling, synthetic aperture radar.

1 Introduction

Automatic interpretation of Synthetic Aperture Radar (SAR) images is an important component of many applications domains such as agriculture [1], urban planning [2], and geology [3]. Segmentation is a crucial step in synthetic aperture radar (SAR) images' automatic interpretation. Due, in part, to the presence of speckle, which can be modeled as strong multiplicative noise, segmentation of SAR images is generally acknowledged as a difficult problem. To cope with the influence of speckle noise on image segmentation, a large number of methods have been proposed. Several edge-based segmentation schemes have been developed. These schemes are based on edge detection filters developed for SAR images with proper modeling of speckle [4], [5], [6], [7]. It has been shown in [8] that the results of these filters depend on the architecture of analyzing windows defined a priori. Furthermore, the problem of forming closed boundaries from separated edge segments given by a filter is difficult and, although many solutions have been proposed, such as morphological closing [7] and the watershed algorithm [9] used in [5], these schemes require postprocessing steps to prevent oversegmentation. Traditional region-based schemes, such as those based on histogram thresholding [10] and region growing [11], have also been used, but they lead to similar limitations. Furthermore, they need speckle reducing techniques [12], [13]. Such schemes instantiate mostly local operations and, thus, lack the robustness and tractability of variational methods [14], [15], particularly those, more recent, based on curve evolution and level sets which have been applied mainly to optical images [16], [17], [18], [19], [20], [21], [22], [23], [24]. For SAR images, a classical snake model [25] is used in [26]. In this region-based scheme, a contour is iteratively deformed to locate the boundary of a region, guided by a statistical criterion. The scheme was shown to improve on the traditional likelihood ratio filter method [4]. The same snake based method was previously used in [27] with different physical noise models. The classical active contour model presents, however, several limitations. First, it discretizes a curve using a set of points and, as a result, topological changes which occur during the evolution of the curve are difficult, if at all possible, to effect. Second, segmentation depends on parameterization and errors in the representation can be significantly amplified during evolution. To extend the classical snake model to multiregion segmentation, another approach based on the statistical polygonal snakes, i.e., a set of nodes joined by segments, is proposed in [28]. This method requires a good initial segmentation to succeed in locating the boundaries of regions. Furthermore, it does not address the segmentation of nonsimply connected regions. Galland et al. [29] generalized polygonal snakes to nonsimply connected regions.

In this study, we use active curves evolution via level sets [30] to segment SAR images into a fixed but arbitrary number N of Gamma-homogeneous regions. Level-sets have the significant advantage of allowing, in a natural and numerically stable manner, variations in the topology of active curves. When the two-region segmentation problem is straightforward to state with active contours and level sets, the extension to an arbitrary fixed number of regions is difficult. The difficulty comes from the fact that, while a simple closed curve unambiguously defines a partition of the image domain into disjoint regions (the interior of the curve and its exterior), the interiors of two or more curves

- *I. Ben Ayed and A. Mitiche are with the Institut National de la Recherche Scientifique, INRS-EMT, 800, de La Gauchetière Ouest, Montréal, QC, H5A 1K6, Canada. E-mail: {benayedi, mitiche}@inrs-emt.uquebec.ca.*
- *Z. Belhadj is with École Supérieure des Communications de Tunis (SUP'COM), Cité Technologique des Communications de Tunis, 2083, Tunisie. E-mail: ziad.belhadj@supcom.rnu.tn.*

Manuscript received 25 May 2004; revised 24 Aug. 2004; accepted 20 Oct. 2004; published online 11 Mar. 2005.
Recommended for acceptance by G. Healey.
For information on obtaining reprints of this article, please send e-mail to: tpami@computer.org, and reference IEEECS Log Number TPAMI-0258-0504.

($N > 2$) may overlap, leading to ambiguous segmentation. To garantee a segmentation that is a partition of the image domain, we use a representation of a partition of the image domain by explicit correspondence between the regions of segmentation and the interior of curves, developed in [20], [21] and demonstrated in the context of motion segmentation and segmentation of optical images. Our SAR functional contains two terms. One term measures the conformity of the data to a Gamma representation. The other is of regularization to obtain regular segmentation boundaries. The minimization of this functional is saught following the Euler-Lagrange descent equations, implemented via curves evolution and level sets.

The remainder of the paper is organized as follows: In the next section, we present the image model. In Section 3, we derive the statistical multiregion criterion in the likelihood sense. Section 4 describes the curve evolution formulation for two-region segmentation, its generalization to multiple regions, and level set implementation. In Section 5, we show experimental results for both synthetic and real images.

2 Image Model

Let $I : \Omega \rightarrow \mathbb{R}^n$ be the intensity SAR image to be segmented, defined on $\Omega \subset \mathbb{R}^2$. The goal of the segmentation process is to derive a partition of the image domain from the image I, i.e., a family $\mathcal{R} = \{\mathbf{R}_i\}_{i\in[1,N]}, \mathbf{R}_i \subset \Omega$ of N subsets of Ω such that they are pairwise disjoint, $\mathbf{R}_i \cap \mathbf{R}_j|_{\forall i \neq j} = \emptyset$, and cover the image domain, $\cup_{i=1}^{N} \mathbf{R}_i = \Omega$, each region being homogeneous with respect to some image characteristics.

When a radar senses a large area, the acquired complex signal is the result of several elementary scatters within a resolution cell. For a single-look SAR image, the intensity is given as $I = a^2 + b^2$, where a and b denote the real and imaginary parts of the complex signal. In the case of multilook SAR images, the L-look intensity is obtained by averaging the L intensity images. Following the *fully developed speckle* hypothesis [31], we model the image in each region $\mathbf{R}_i, (i \in [1, N])$ by a Gamma distribution of mean intensity $\mu_{\mathbf{R}_i}$ and a number L of looks:

$$P_{\mu_{\mathbf{R}_i},L}(I(\mathbf{x})) = \frac{L^L}{\mu_{\mathbf{R}_i}\Gamma(L)}\left(\frac{I(\mathbf{x})}{\mu_{\mathbf{R}_i}}\right)^{L-1} e^{-\frac{LI(\mathbf{x})}{\mu_{\mathbf{R}_i}}}. \tag{1}$$

The image in each region $\mathbf{R}_i, (i \in [1, N])$ is therefore characterized by its mean $\mu_{\mathbf{R}_i}$ and the number of looks L, which we take to be the same for all regions. The distribution given by (1) reduces to the exponential distribution in the 1-look case. This model has been extensively used in SAR image applications such as speckle reduction [13], edge detection [4], and segmentation [28], [29], [5], [26].

3 Segmentation Criterion

Assuming that $I(\mathbf{x})$ is independent of $I(\mathbf{y})$ for $\mathbf{x} \neq \mathbf{y}$, the problem of segmentation consists of finding the family of regions $\hat{\mathcal{R}}$ that maximizes the likelihood $\mathcal{L}(\mathcal{R}|I)$:

$$\begin{aligned}\hat{\mathcal{R}} &= \arg\max_{\mathcal{R}} \mathcal{L}(\mathcal{R}|I) \\ &= \arg\max_{\mathcal{R}} \prod_{\mathbf{x}\in\mathbf{R}_1} P_{\mu_{\mathbf{R}_1},L}(I(\mathbf{x})) \prod_{\mathbf{x}\in\mathbf{R}_2} P_{\mu_{\mathbf{R}_2},L}(I(\mathbf{x})) \cdots \prod_{\mathbf{x}\in\mathbf{R}_N} P_{\mu_{\mathbf{R}_N},L}(I(\mathbf{x})).\end{aligned} \tag{2}$$

Maximizing $\mathcal{L}$ is equivalent to minimizing $-\log(\mathcal{L})$. If we estimate $\mu_{\mathbf{R}}$ by the average of I inside $\mathbf{R}$ for all $\mathbf{R} \in \mathcal{R}$, i.e., if we take:

$$\mu_{\mathbf{R}} = \frac{\int_{\mathbf{R}} I(\mathbf{x})\, d\mathbf{x}}{\int_{\mathbf{R}} d\mathbf{x}}, \tag{3}$$

then, following the computation in [29], using (1), and after some algebraic manipulations, we obtain:

$$-\log(\mathcal{L}(\mathcal{R}|I)) = L\sum_{i=1}^{N} a_{\mathbf{R}_i}.\log\mu_{\mathbf{R}_i} + c(L, I), \tag{4}$$

where $c(L, I)$ is a constant which depends only on the image and the number of looks and, therefore, is independent of the segmentation, and $a_{\mathbf{R}}$ denotes the area of $\mathbf{R}$ for $\mathbf{R} \in \mathcal{R}$:

$$a_{\mathbf{R}} = \int_{\mathbf{R}} d\mathbf{x}. \tag{5}$$

The problem to solve becomes to determine $\hat{\mathcal{R}}$ that minimizes the following segmentation criterion:

$$\mathcal{C} = \sum_{i=1}^{N} a_{\mathbf{R}_i}.\log\mu_{\mathbf{R}_i}. \tag{6}$$

We note that this functional is independent of the number of looks and that the means and areas depend on the segmentation and, consequently, are to be estimated along with the segmentation process. In the next section, we will solve the minimization of (6) by curve evolution, through the associated Euler-Lagrange descent equations implemented robustly via level sets. We first treat the case of segmentation into two regions (Section 4.1), which we subsequently generalize to a fixed but otherwise arbitrary number of regions (Section 4.2).

4 Solution by Curves Evolution

4.1 Two-Region Segmentation

To solve the problem of minimizing $\mathcal{C}$ by curve evolution in the case of two regions, we consider a simple closed planar curve $\vec{\gamma}(s) : [0, 1] \rightarrow \Omega$ parameterized by arc parameter $s \in [0, 1]$, and we associate its interior to region $\mathbf{R}_1$: $\mathbf{R}_1 = \mathbf{R}_{\vec{\gamma}}$ and its exterior to $\mathbf{R}_2$: $\mathbf{R}_2 = \mathbf{R}_1^c$. The Euler-Lagrange descent equation corresponding to $\mathcal{C}$ is obtained by embedding the curve $\vec{\gamma}$ into a family of one-parameter curves $\vec{\gamma}(s, t) : [0, 1] \times \mathbb{R}^+ \rightarrow \Omega$ and solving the partial differential equation:

$$\frac{d\vec{\gamma}}{dt} = -\frac{\partial\mathcal{C}}{\partial\vec{\gamma}}, \tag{7}$$

where $\frac{\partial\mathcal{C}}{\partial\vec{\gamma}}$ denotes the functional derivative of the functional $\mathcal{C}$ with respect to curve $\vec{\gamma}$. The segmentation is defined by

the partition $\mathcal{R} = \{\mathbf{R}_1, \mathbf{R}_2\}$ at convergence, i.e., when $t \to \infty$. We have:

$$\frac{\partial \mathcal{C}}{\partial \vec{\gamma}} = \frac{\partial (a_{\mathbf{R}_1} \log \mu_{\mathbf{R}_1} + a_{\mathbf{R}_2} \log \mu_{\mathbf{R}_2})}{\partial \vec{\gamma}} = \log \mu_{\mathbf{R}_1} \frac{\partial a_{\mathbf{R}_1}}{\partial \vec{\gamma}} + \frac{a_{\mathbf{R}_1}}{\mu_{\mathbf{R}_1}} \frac{\partial \mu_{\mathbf{R}_1}}{\partial \vec{\gamma}} + \log \mu_{\mathbf{R}_2} \frac{\partial a_{\mathbf{R}_2}}{\partial \vec{\gamma}} + \frac{a_{\mathbf{R}_2}}{\mu_{\mathbf{R}_2}} \frac{\partial \mu_{\mathbf{R}_2}}{\partial \vec{\gamma}}. \tag{8}$$

Using the result in [14] which shows that, for a scalar function f, the functional derivative with respect to curve $\vec{\gamma}$ of $\int_{\mathbf{R}_{\vec{\gamma}}} f(\mathbf{x}) d\mathbf{x}$ is $f\vec{n}$, where $\vec{n}$ is the external unit normal of $\vec{\gamma}$, we have:

$$\frac{\partial a_{\mathbf{R}_1}}{\partial \vec{\gamma}} = \vec{n} \qquad \frac{\partial a_{\mathbf{R}_2}}{\partial \vec{\gamma}} = -\vec{n} \tag{9}$$

and, with the notation $s_{\mathbf{R}} = \int_{\mathbf{R}} I(\mathbf{x})\, d\mathbf{x}\ \forall \mathbf{R} \in \mathcal{R}$, we also have:

$$\frac{\partial \mu_{\mathbf{R}_1}}{\partial \vec{\gamma}} = \frac{\partial \left(\frac{s_{\mathbf{R}_1}}{a_{\mathbf{R}_1}}\right)}{\partial \vec{\gamma}} = \frac{a_{\mathbf{R}_1} \nabla s_{\mathbf{R}_1} - s_{\mathbf{R}_1} \nabla a_{\mathbf{R}_1}}{a_{\mathbf{R}_1}^2} = \frac{(I - \mu_{\mathbf{R}_1})}{a_{\mathbf{R}_1}} \vec{n}$$
$$\frac{\partial \mu_{\mathbf{R}_2}}{\partial \vec{\gamma}} = \frac{\partial \left(\frac{s_{\mathbf{R}_2}}{a_{\mathbf{R}_2}}\right)}{\partial \vec{\gamma}} = \frac{a_{\mathbf{R}_2} \nabla s_{\mathbf{R}_2} - s_{\mathbf{R}_2} \nabla a_{\mathbf{R}_2}}{a_{\mathbf{R}_2}^2} = -\frac{(I - \mu_{\mathbf{R}_2})}{a_{\mathbf{R}_2}} \vec{n}. \tag{10}$$

Note that the minus sign in the second equation of (10) is due to the fact that $\vec{n}$, being the external unit normal of the boundary of $\mathbf{R}_1$, the external unit normal of the boundary of its complement, $\mathbf{R}_2$, is $-\vec{n}$. By substituting (9) and (10) into (8) and after some algebraic manipulations, we arrive at the evolution equation for curve $\vec{\gamma}$:

$$\frac{d\vec{\gamma}}{dt} = -(\log \mu_{\mathbf{R}_1} + \frac{I}{\mu_{\mathbf{R}_1}} - \log \mu_{\mathbf{R}_2} - \frac{I}{\mu_{\mathbf{R}_2}})\vec{n}, \tag{11}$$

which will define the segmentation at convergence, i.e., when $t \to \infty$.

In order to avoid the occurrence of small, isolated regions in the final segmentation, we add to $\mathcal{C}$ a regularization term $\mathcal{S}(\vec{\gamma})$ which is defined related to the length of the curve $\vec{\gamma}$:

$$\mathcal{S}(\vec{\gamma}) = \lambda \oint_{\vec{\gamma}} ds, \tag{12}$$

where λ is a positive real constant to weigh the contribution of $\mathcal{S}$ against $\mathcal{C}$. The derivative of $\mathcal{S}(\vec{\gamma})$ with respect to $\vec{\gamma}$ is:

$$\frac{\partial \mathcal{S}(\vec{\gamma})}{\partial \vec{\gamma}} = -\lambda \kappa \vec{n}, \tag{13}$$

where κ is the mean curvature function of $\vec{\gamma}$. With this regularization term, the final evolution equation for $\vec{\gamma}$ is:

$$\frac{d\vec{\gamma}}{dt} = -\left(\log \mu_{\mathbf{R}_1} + \frac{I}{\mu_{\mathbf{R}_1}} - \log \mu_{\mathbf{R}_2} - \frac{I}{\mu_{\mathbf{R}_2}} + \lambda \kappa\right)\vec{n}. \tag{14}$$

4.2 Generalization to Multiple Region Segmentation

4.2.1 Representation of a Partition

For segmentation into multiple regions, i.e., into a fixed but arbitrary number of regions, we consider a family $\vec{\gamma}_i : [0,1] \to \Omega, i = 1, \ldots, N-1$ of plane curves parametrized by the arc parameter $s \in [0,1]$. As mentioned in Section 1, the use of two or more curves required for the segmentation of N regions, with $N > 2$, may lead to ambiguous segmentation results when the interior of curves overlap. To guarantee an unambiguous segmentation, i.e., a partition of the image domain Ω, we use the following explicit correspondence between the family $\{\mathbf{R}_{\vec{\gamma}_i}\}$ of regions enclosed by the curves $\{\vec{\gamma}_i\}$ and the regions of partition $\mathcal{R} = \{\mathbf{R}_i\}_{i \in [1,N]}$ of the image domain Ω [20], [21]:

$$\begin{aligned}
&\mathbf{R}_1 = \mathbf{R}_{\vec{\gamma}_1} \\
&\mathbf{R}_2 = \mathbf{R}^c_{\vec{\gamma}_1} \cap \mathbf{R}_{\vec{\gamma}_2} \\
&\cdots \\
&\mathbf{R}_k = \mathbf{R}^c_{\vec{\gamma}_1} \cap \mathbf{R}^c_{\vec{\gamma}_2} \cap \cdots \cap \mathbf{R}^c_{\vec{\gamma}_{k-1}} \cap \mathbf{R}_{\vec{\gamma}_k} \\
&\cdots \\
&\mathbf{R}_N = \mathbf{R}^c_{\vec{\gamma}_1} \cap \mathbf{R}^c_{\vec{\gamma}_2} \cap \cdots \cap \mathbf{R}^c_{\vec{\gamma}_{k-1}} \cap \mathbf{R}^c_{\vec{\gamma}_{N-1}}
\end{aligned} \tag{15}$$

for any family of plane curves $(\vec{\gamma}_i)_{i=1}^{N-1}$, the family $\{\mathbf{R}_i\}_{i \in [1,N]}$ thus obtained is, by construction, a partition of the image domain. The partition representation is shown in Fig. 1 for five regions. Under this representation of a partition, we will now write our curve evolution equations for segmentation into a fixed but arbitrary number of regions.

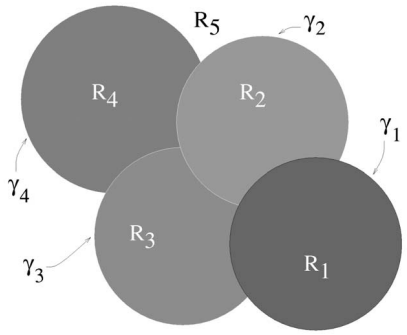

Fig. 1. Representation of a five-region partition.

4.2.2 Curve Evolution Equations

With the above choice of representing a partition of the image domain into N regions and with a regularization term related to the length of curves, the criterion to minimize is:

$$\mathcal{C} = \sum_{i=1}^{N} a_{\mathbf{R}_i} . \log \mu_{\mathbf{R}_i} + \sum_{i=1}^{N} \mathcal{S}(\vec{\gamma}_i). \tag{16}$$

To compute the functional derivatives $\frac{\delta \mathcal{C}}{\delta \vec{\gamma}_i}$, we start with $\vec{\gamma}_1$ and we rewrite the areas and the means appearing in the the criterion $\mathcal{C}$ as follows:

$$\begin{aligned}
a_{\mathbf{R}_1} &= \int_{\mathbf{R}_{\vec{\gamma}_1}} d\mathbf{x} \\
a_{\mathbf{R}_2} &= \int_{\mathbf{R}^c_{\vec{\gamma}_1}} \chi_{\mathbf{R}_{\vec{\gamma}_2}} d\mathbf{x} \\
&\cdots \\
a_{\mathbf{R}_k} &= \int_{\mathbf{R}^c_{\vec{\gamma}_1}} \chi_{\mathbf{R}^c_{\vec{\gamma}_2}} \cdots \chi_{\mathbf{R}^c_{\vec{\gamma}_{k-1}}} \chi_{\mathbf{R}_{\vec{\gamma}_k}} d\mathbf{x} \\
&\cdots
\end{aligned}$$

$$
\begin{aligned}
a_{\mathbf{R}_N} &= \int_{\mathbf{R}^c_{\vec{\gamma}_1}} \chi_{\mathbf{R}^c_{\vec{\gamma}_2}} \cdots \chi_{\mathbf{R}^c_{\vec{\gamma}_k}} \cdots \chi_{\mathbf{R}^c_{\vec{\gamma}_{N-1}}} d\mathbf{x} \\
s_{\mathbf{R}_1} &= \int_{\mathbf{R}_{\vec{\gamma}_1}} I(\mathbf{x}) d\mathbf{x} \\
s_{\mathbf{R}_2} &= \int_{\mathbf{R}^c_{\vec{\gamma}_1}} \chi_{\mathbf{R}_{\vec{\gamma}_2}} I(\mathbf{x}) d\mathbf{x} \\
&\cdots \\
s_{\mathbf{R}_k} &= \int_{\mathbf{R}^c_{\vec{\gamma}_1}} \chi_{\mathbf{R}^c_{\vec{\gamma}_2}} \cdots \chi_{\mathbf{R}^c_{\vec{\gamma}_{k-1}}} \chi_{\mathbf{R}_{\vec{\gamma}_k}} I(\mathbf{x}) d\mathbf{x} \\
&\cdots \\
s_{\mathbf{R}_N} &= \int_{\mathbf{R}^c_{\vec{\gamma}_1}} \chi_{\mathbf{R}^c_{\vec{\gamma}_2}} \cdots \chi_{\mathbf{R}^c_{\vec{\gamma}_k}} \cdots \chi_{\mathbf{R}^c_{\vec{\gamma}_{N-1}}} I(\mathbf{x}) d\mathbf{x} \\
\mu_{\mathbf{R}} &= \frac{s_{\mathbf{R}}}{a_{\mathbf{R}}} \forall \mathbf{R} \in \mathcal{R},
\end{aligned}
\tag{17}
$$

where $\chi_{\mathbf{R}}$ is the characteristic function of $\mathbf{R}$, i.e., $\chi_{\mathbf{R}} = 1$ if $\mathbf{x} \in \mathbf{R}$ and $\chi_{\mathbf{R}} = 0$ if $\mathbf{x} \in \mathbf{R}^c$. Using the same computation method as in Section 4.1, we derive each term in the first sum in $\mathcal{C}$ as follows:

$$
\begin{aligned}
\frac{\partial a_{\mathbf{R}_1} \log \mu_{\mathbf{R}_1}}{\partial \vec{\gamma}_1} &= (\xi_{\mathbf{R}_1} - 1)\vec{n_1} \\
\frac{\partial a_{\mathbf{R}_2} \log \mu_{\mathbf{R}_2}}{\partial \vec{\gamma}_1} &= -\chi_{\mathbf{R}_{\vec{\gamma}_2}} (\xi_{\mathbf{R}_2} - 1)\vec{n_1} \\
&\cdots \\
\frac{\partial a_{\mathbf{R}_k} \log \mu_{\mathbf{R}_k}}{\partial \vec{\gamma}_1} &= -\chi_{\mathbf{R}^c_{\vec{\gamma}_2}} \cdots \chi_{\mathbf{R}^c_{\vec{\gamma}_{k-1}}} \chi_{\mathbf{R}_{\vec{\gamma}_k}} (\xi_{\mathbf{R}_k} - 1)\vec{n_1} \\
&\cdots \\
\frac{\partial a_{\mathbf{R}_N} \log \mu_{\mathbf{R}_N}}{\partial \vec{\gamma}_1} &= -\chi_{\mathbf{R}^c_{\vec{\gamma}_2}} \cdots \chi_{\mathbf{R}^c_{\vec{\gamma}_k}} \cdots \chi_{\mathbf{R}^c_{\vec{\gamma}_{N-1}}} (\xi_{\mathbf{R}_N} - 1)\vec{n_1},
\end{aligned}
\tag{18}
$$

where

$$
\xi_{\mathbf{R}} = \log \mu_{\mathbf{R}} + \frac{I}{\mu_{\mathbf{R}}} \forall \mathbf{R} \in \mathcal{R} \tag{19}
$$

and $\vec{n_1}$ is the outward unit normal to $\vec{\gamma}_1$. Since $\sum_{j=2}^{N-1} \oint_{\vec{\gamma}_j} ds$ has no functional dependence on $\vec{\gamma}_1$, the functional derivative of the second sum in $\mathcal{C}$ is:

$$
\frac{\partial \sum_{j=1}^{N-1} \oint_{\vec{\gamma}_j} ds}{\partial \vec{\gamma}_1} = \frac{\partial \oint_{\vec{\gamma}_1} ds}{\partial \vec{\gamma}_1} = \lambda \kappa_1 \vec{n_1}. \tag{20}
$$

Because $\{\mathbf{R}_{\vec{\gamma}_2}, \mathbf{R}^c_{\vec{\gamma}_2} \cap \mathbf{R}_{\vec{\gamma}_3}, \mathbf{R}^c_{\vec{\gamma}_2} \cap \mathbf{R}^c_{\vec{\gamma}_3} \cap \mathbf{R}_{\vec{\gamma}_4}, \ldots, \mathbf{R}^c_{\vec{\gamma}_2} \cap \cdots \cap \mathbf{R}^c_{\vec{\gamma}_{k-1}} \cap \mathbf{R}^c_{\vec{\gamma}_{N-1}}\}$ is a partition, we have:

$$
1 = \chi_{\mathbf{R}_{\vec{\gamma}_2}} + \chi_{\mathbf{R}^c_{\vec{\gamma}_2}} \cdot \chi_{\mathbf{R}_{\vec{\gamma}_3}} + \cdots + \chi_{\mathbf{R}^c_{\vec{\gamma}_2}} \cdot \chi_{\mathbf{R}^c_{\vec{\gamma}_3}} \cdots \chi_{\mathbf{R}^c_{\vec{\gamma}_{N-1}}}. \tag{21}
$$

This identity simplifies the sum of the N equations in (18) and the curvature equation (20), to give the following evolution equation of the curve $\vec{\gamma}_1$:

$$
\frac{d\vec{\gamma}_1(s,t)}{dt} = [\xi_1(\vec{\gamma}_1(s,t)) - \Phi_1(\vec{\gamma}_1(s,t)) + \lambda \kappa_1(s,t)]\vec{n}_1(s,t), \tag{22}
$$

where Φ_1 is defined for all $\mathbf{x} \in \Omega$ by:

$$
\begin{aligned}
\Phi_1(\mathbf{x}) = {} & \xi_{\mathbf{R}_2}(\mathbf{x}) \chi_{\mathbf{R}_{\vec{\gamma}_2}}(\mathbf{x}) + \xi_{\mathbf{R}_3}(\mathbf{x}) \chi_{\mathbf{R}^c_{\vec{\gamma}_2}}(\mathbf{x}) \chi_{\mathbf{R}_{\vec{\gamma}_3}}(\mathbf{x}) + \ldots \\
& + \xi_{\mathbf{R}_{N-1}} \chi_{\mathbf{R}^c_{\vec{\gamma}_3}}(\mathbf{x}) \ldots \chi_{\mathbf{R}^c_{\vec{\gamma}_{N-2}}}(\mathbf{x}) \chi_{\mathbf{R}_{\vec{\gamma}_{N-1}}}(\mathbf{x}) \\
& + \xi_{\mathbf{R}_N}(\mathbf{x}) \chi_{\mathbf{R}^c_{\vec{\gamma}_2}}(\mathbf{x}) \chi_{\mathbf{R}^c_{\vec{\gamma}_3}}(\mathbf{x}) \ldots \chi_{\mathbf{R}^c_{\vec{\gamma}_{N-2}}}(\mathbf{x}) \chi_{\mathbf{R}^c_{\vec{\gamma}_{N-1}}}(\mathbf{x}).
\end{aligned}
$$

Using

$$
1 = \chi_{\mathbf{R}_{\vec{\gamma}_j}} + \chi_{\mathbf{R}^c_{\vec{\gamma}_j}} \cdot \chi_{\mathbf{R}_{\vec{\gamma}_{j+1}}} + \cdots + \chi_{\mathbf{R}^c_{\vec{\gamma}_j}} \cdot \chi_{\mathbf{R}^c_{\vec{\gamma}_{j+1}}} \ldots \chi_{\mathbf{R}^c_{\vec{\gamma}_{N-1}}} \ \forall j \tag{23}
$$

because $\{\mathbf{R}_{\vec{\gamma}_j}, \mathbf{R}^c_{\vec{\gamma}_j} \cap \mathbf{R}_{\vec{\gamma}_{j+1}}, \mathbf{R}^c_{\vec{\gamma}_j} \cap \mathbf{R}^c_{\vec{\gamma}_{j+1}} \cap \mathbf{R}_{\vec{\gamma}_{j+2}}, \ldots, \mathbf{R}^c_{\vec{\gamma}_j} \cap \cdots \cap \mathbf{R}^c_{\vec{\gamma}_{k-1}} \cap \mathbf{R}^c_{\vec{\gamma}_{N-1}}\}$ is a partition for all j, and proceeding similarly to compute the functional derivatives $\frac{\delta \mathcal{C}}{\delta \vec{\gamma}_j}$ for all j, the Euler-Lagrange descent equations of the curves evolution for the minimization of the criterion $\mathcal{C}$ are given by:

$$
\begin{aligned}
\frac{d\vec{\gamma}_1}{dt} &= -(\xi_{\mathbf{R}_1}(\vec{\gamma}_1) - \Phi_1(\vec{\gamma}_1) + \lambda \kappa_1)\vec{n}_1 \\
\frac{d\vec{\gamma}_2}{dt} &= -(\chi_{\mathbf{R}^c_1}(\vec{\gamma}_2)[\xi_{\mathbf{R}_2}(\vec{\gamma}_2) - \Phi_2(\vec{\gamma}_2)] + \lambda \kappa_2)\vec{n}_2 \\
&\cdots \\
\frac{d\vec{\gamma}_j}{dt} &= -(\chi_{\mathbf{R}^c_1}(\vec{\gamma}_j) \cdots \chi_{\mathbf{R}^c_{j-1}}(\vec{\gamma}_j)[\xi_{\mathbf{R}_j}(\vec{\gamma}_j) - \Phi_j(\vec{\gamma}_j)] + \lambda \kappa_j)\vec{n}_j \\
&\cdots \\
\frac{d\vec{\gamma}_{N-1}}{dt} &= -(\chi_{\mathbf{R}^c_1}(\vec{\gamma}_{N-1}) \cdots \chi_{\mathbf{R}^c_{N-2}}(\vec{\gamma}_{N-1})[\xi_{\mathbf{R}_{N-1}}(\vec{\gamma}_{N-1}) \\
&\quad - \Phi_{N-1}(\vec{\gamma}_{N-1})] + \lambda \kappa_{N-1})\vec{n}_{N-1},
\end{aligned}
\tag{24}
$$

where $\vec{n}_j$ is the outward unit normal to $\vec{\gamma}_j$, κ_j is the curvature function of $\vec{\gamma}_j$, for $j = 1, \ldots, N-1$, and Φ_j is defined for all $\mathbf{x} \in \Omega$ by:

$$
\begin{aligned}
\Phi_j(\mathbf{x}) = {} & \xi_{\mathbf{R}_{j+1}}(\mathbf{x}) \chi_{\mathbf{R}_{\vec{\gamma}_{j+1}}}(\mathbf{x}) + \xi_{\mathbf{R}_{j+2}}(\mathbf{x}) \chi_{\mathbf{R}^c_{\vec{\gamma}_{j+1}}}(\mathbf{x}) \chi_{\mathbf{R}_{\vec{\gamma}_{j+2}}}(\mathbf{x}) + \ldots \\
& + \xi_{\mathbf{R}_{N-1}}(\mathbf{x}) \chi_{\mathbf{R}^c_{\vec{\gamma}_{j+1}}}(\mathbf{x}) \ldots \chi_{\mathbf{R}^c_{\vec{\gamma}_{N-2}}}(\mathbf{x}) \chi_{\mathbf{R}_{\vec{\gamma}_{N-1}}}(\mathbf{x}) \\
& + \xi_{\mathbf{R}_N}(\mathbf{x}) \chi_{\mathbf{R}^c_{\vec{\gamma}_{j+1}}}(\mathbf{x}) \ldots \chi_{\mathbf{R}^c_{\vec{\gamma}_{N-2}}}(\mathbf{x}) \chi_{\mathbf{R}^c_{\vec{\gamma}_{N-1}}}(\mathbf{x}).
\end{aligned}
$$

4.3 Level-Set Implementation

We use the level-set formalism [32] to implement the system of curves evolution equations (24). The level-set representation has well-known advantages over an explicit representation such as snakes [30]. There are indeed several problems with an explicit representation. First, topological changes, which occur during evolution, are difficult if at all possible to effect. Second, results depend on parametrization and errors in representation can significantly compound during evolution. In contrast, a level sets representation allows topological changes in a natural way and can be implemented by stable numerical schemes. With level-sets, curve $\vec{\gamma}_j$ is represented implicitly by the zero level set of a function $u_j : \mathbb{R}^2 \to \mathbb{R}$ (with $j = 1, \ldots, N-1$), i.e., we define $\vec{\gamma}_j$ as the set where $u_j = 0$, with the convention that $u_j > 0$ inside $\vec{\gamma}_j$ and $u_j < 0$ outside $\vec{\gamma}_j$. Then,

$$
\vec{n}_j = \frac{\vec{\nabla} u_j}{\|\vec{\nabla} u_j\|} \tag{25}
$$

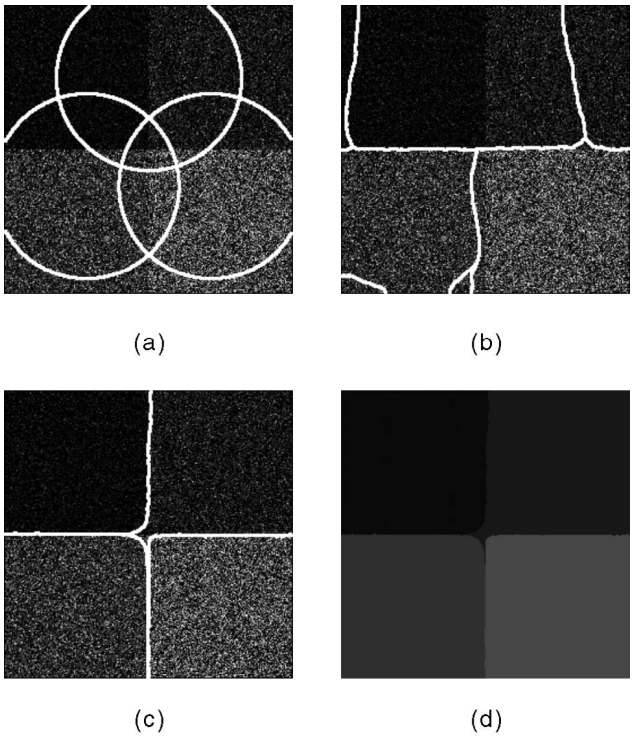

Fig. 2. Synthetic 1-look white speckle image of four regions: (a) initial curves, (b) intermediate curves, (c) final positions, and (d) computed segmentation.

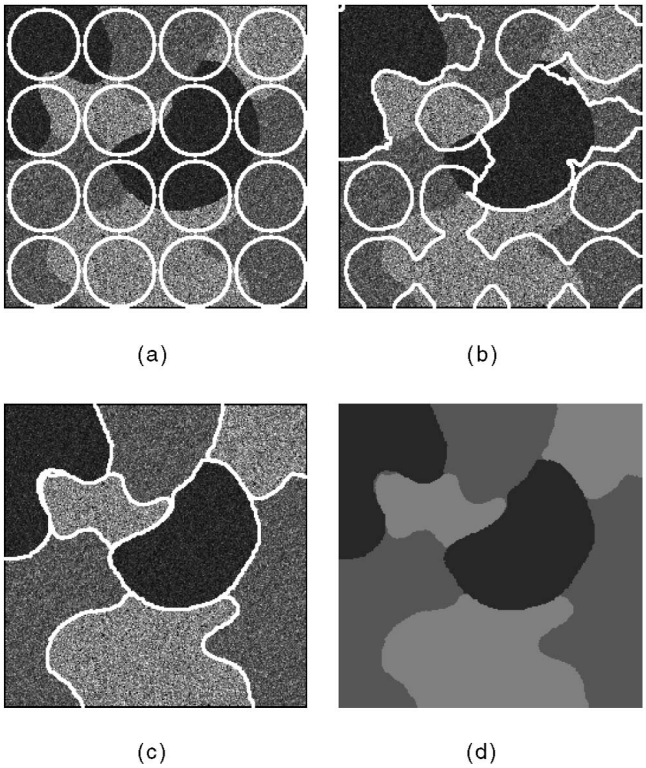

Fig. 3. Synthetic 8-look image of three regions: (a) initial curves, (b) intermediate curves, (c) final positions, and (d) computed segmentation.

and the curve $\vec{\gamma}_j$ may change topology while u_j remains a function. For a point $\mathbf{x} \in \vec{\gamma}_j$, we have: $u_j(\mathbf{x}, t) = 0 \ \forall t$. This implies that

$$\frac{du_j(\mathbf{x},t)}{dt} = \frac{\partial u_j}{\partial t}(\mathbf{x},t) + \vec{\nabla} u_j \cdot \frac{d\vec{\gamma}_j}{dt} = 0. \tag{26}$$

Using (25) and (26), the evolution equation of the form $\frac{d\vec{\gamma}_j}{dt} = F\vec{n}_j$ leads to the level-set equation of the form $\frac{\partial u_j}{\partial t}(\mathbf{x},t) = -F\|\vec{\nabla} u_j\|$. The level-set evolution equations corresponding to (24) are then given by the following system of coupled partial differential equations:

$$\begin{aligned}
\frac{\partial u_1}{\partial t}(\mathbf{x},t) &= -\left(\xi_{\mathbf{R}_1}(\mathbf{x}) - \Phi_1(\mathbf{x}) + \lambda\kappa_{u_1}\right)\|\vec{\nabla} u_1(\mathbf{x},t)\| \\
&\cdots \\
\frac{\partial u_j}{\partial t}(\mathbf{x},t) &= -\left(\chi_{\{u_1(\mathbf{x},t)\le 0\}} \cdots \chi_{\{u_{j-1}(x,t)\le 0\}}[\xi_{\mathbf{R}_j}(\mathbf{x}) - \Phi_j(\mathbf{x})]\right. \\
&\quad \left. + \lambda\kappa_{u_j}\right)\|\vec{\nabla} u_j(\mathbf{x},t)\| \\
&\cdots \\
\frac{\partial u_{N-1}}{\partial t}(\mathbf{x},t) &= -\left(\chi_{\{u_1(\mathbf{x},t)\le 0\}} \cdots \chi_{\{u_{N-2}(\mathbf{x},t)\le 0\}}[\xi_{\mathbf{R}_{N-1}}(\mathbf{x})\right. \\
&\quad \left. - \Phi_{N-1}(\mathbf{x})] + \lambda\kappa_{u_{N-1}}\right)\|\vec{\nabla} u_{N-1}(\mathbf{x},t)\|,
\end{aligned} \tag{27}$$

where $\chi_{\{u_k(\mathbf{x},t)\le 0\}} = 1$ if $u_k(\mathbf{x},t) \le 0$ and 0 otherwise, and κ_{u_j} is the curvature of the zero level-set of u_j with κ_u being given as a function of u by:

$$\kappa_u = -\vec{\nabla} \cdot \left(\vec{\nabla} u / \|\vec{\nabla} u\|\right). \tag{28}$$

The positive weight λ of the curvature term is set experimentally. Defining $\mathbf{R}_{u_i}(t) = \{\mathbf{x} \in \Omega | u_i(\mathbf{x},t) > 0\}, \quad i = 1, \ldots, N-1$, the segmentation is then given as $t \to \infty$ by the family: $\{\mathbf{R}_{u_1}(t),\ \mathbf{R}_{u_1}(t)^c \cap \mathbf{R}_{u_2}(t),\ \mathbf{R}_{u_1}(t)^c \cap \mathbf{R}_{u_2}(t)^c \cap \mathbf{R}_{u_3}(t) \ldots (\cup_{j=1}^{N-1}\mathbf{R}_{u_j}(t))^c\}$. Discretization of level-set equations is detailed in [30]. We should note that the evolution equation for a curve $\vec{\gamma}_j$ is only valid for points on the curve $\mathbf{x} \in \vec{\gamma}_j$. However, with the representation of partition we use, we can extend this equation to the evolution of u_j over Ω.

5 Experimental Results

To verify the SAR image intensity model and the segmentation method we proposed, we first simulate a 1-look case by the synthetic image of Fig. 2. It consists of four regions, as visual inspection can quickly indicate. It has been obtained by multiplying a perfect reflectivity synthetic image by a white exponential speckle noise. We simulated the 8-look case by the synthetic image of Fig. 3. It contains three regions and it is obtained by averaging the intensities of a 1-look synthetic image. Fig. 2a and Fig. 3a show the initial position of the evolving curves for the two images, Fig. 2b and Fig. 3b show an intermediate position of these curves, Fig. 2c and Fig. 3c show final position, and, finally, Fig. 2d and Fig. 3d display the segmented regions represented by their mean gray value at convergence. Initial curves in Fig. 2a are represented by circles in the middle of the image to illustrate the fact that the result is independent of the initialization. Regions in the 8-look simulated image have disjoint components to illustrate the ability of the algorithm

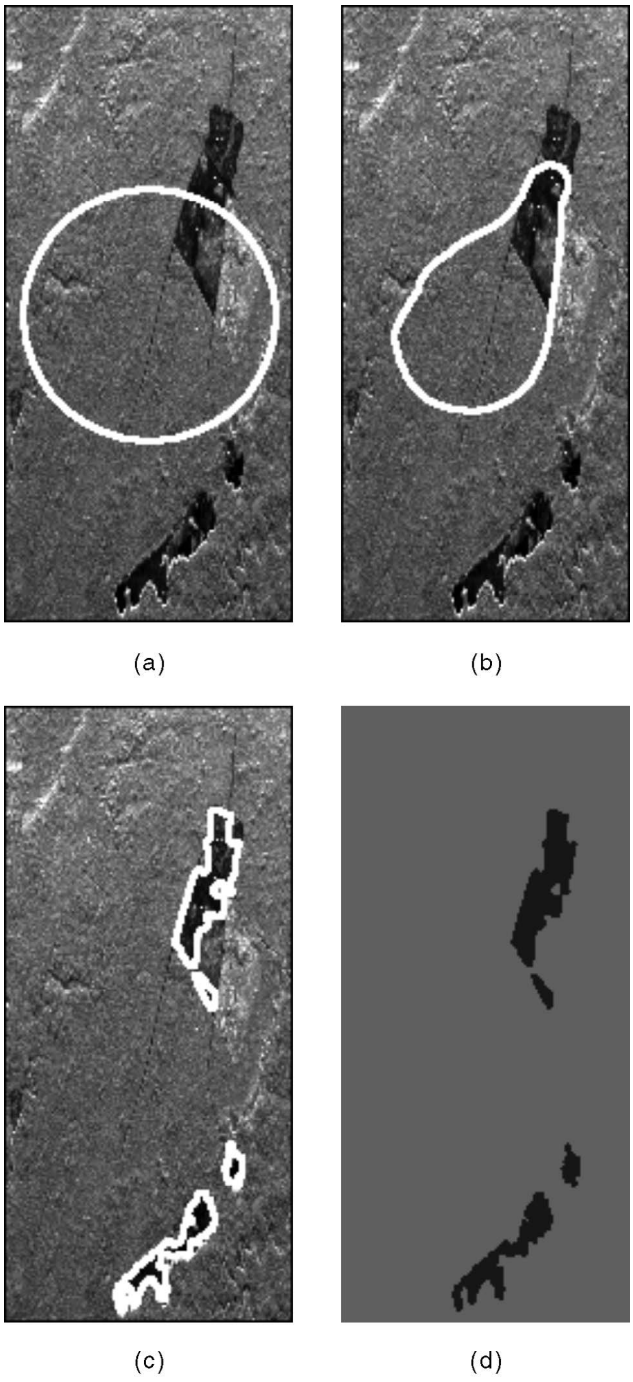

Fig. 4. Belize SAR image: (a) initial curves, (b) intermediate curves, (c) final positions, and (d) computed segmentation.

to handle automatically topological changes of curves. The regularization parameter was set to 0.2 for the simulation of Fig. 2 and to 0.1 for the simulation of Fig. 3. The computational time depends on the initialization and the size of the image. On a 1.7 MHZ PC, the algorithm needed 954s to process the 256×256 pixels to produce the result of Fig. 2, but only 246s to produce the same number of pixels in the simulation of Fig. 3. Indeed, the initialization of Fig. 3 is closer to the result than the initialization of Fig. 2. Results of both segmentations are conform to expectation. We also experimented with a real 16-look NASA/JPL SAR image of the Belize region, shown in Fig. 4. Finally, we applied the

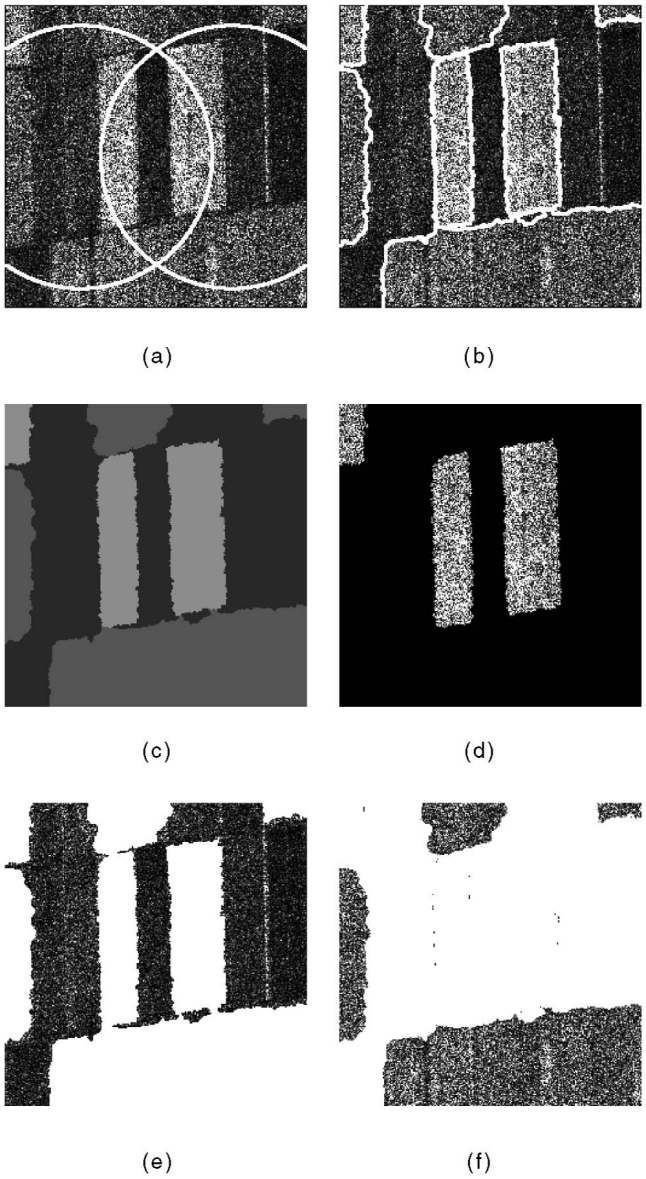

Fig. 5. ERS SAR image: (a) initial curves, (b) final positions, (c) computed segmentation, and (d), (e), and (f) regions segmentation.

algorithm to an ERS-1 intensity 1-look real SAR image of an agricultural scene and to the high speckle noise 1-look NASA/JPL SAR image of the Landes forest shown, respectively, in Fig. 5 and Fig. 6. We segmented the Belize image into two regions, the ERS image into three regions, and the Landes forest image into three regions (the choice of the number of regions is based on visual inspection). The regularization parameter was set to 0.1 for the Belize image and to 0.2 for the ERS image and the Landes forest image. The algorithm needed 183s to process the 128×274 pixels of the Belize image, 907s to process the 250×250 pixels of the ERS image, and 1848s to process the 771×445 pixels of the Landes forest image. We show regions corresponding to segmentations in Figs. 5d, 5e, 5f, 6d, 6e, and 6f. All results show an excellent performance of the method. Despite the level of speckle in the Landes forest image, the method succeeded in locating the boundaries of the fine linear structures which appear in the image.

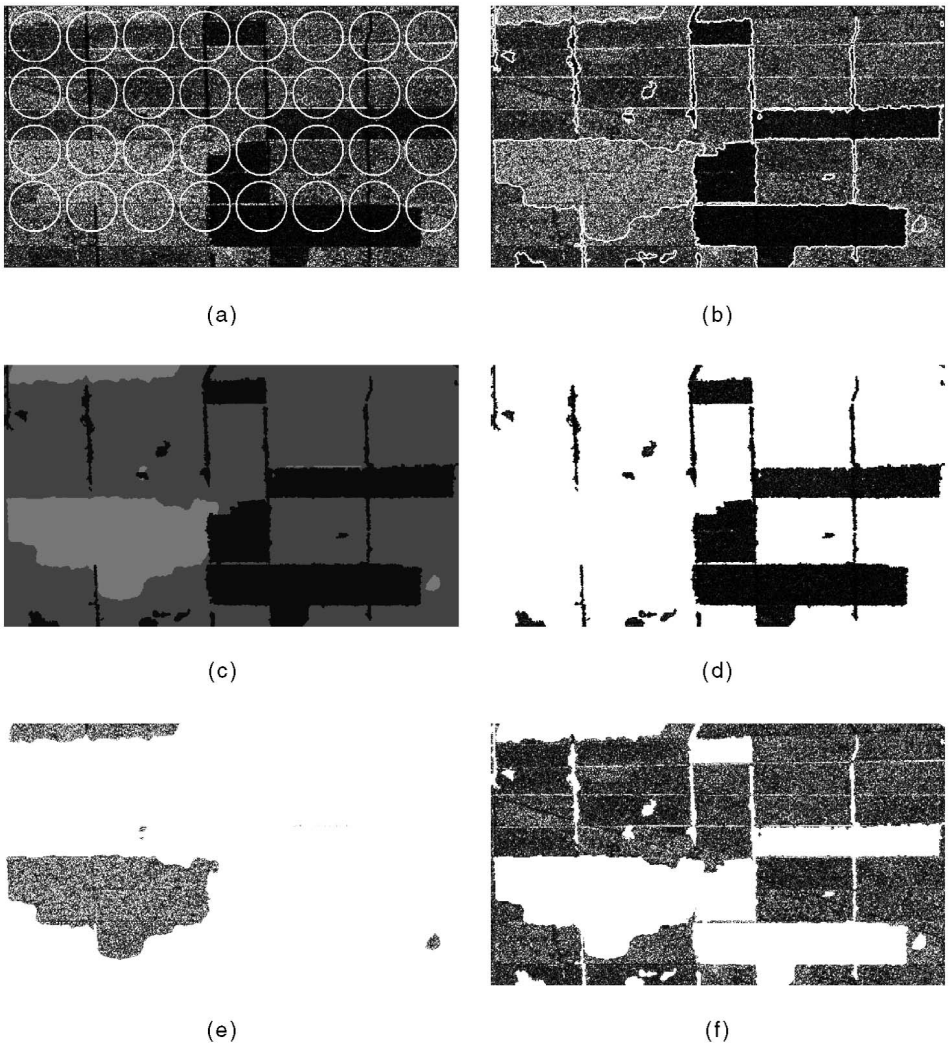

Fig. 6. Landes SAR image: (a) initial curves, (b) final positions, (c) computed segmentation, and (d), (e), and (f) regions segmentation.

6 Conclusion

We presented a curve evolution algorithm for segmenting a synthetic aperture radar (SAR) image into a fixed but arbitrary number of Gamma-homogeneous regions. This algorithm consists in evolving curves in order to minimize a statistical criterion. This led to partitions of the image domain following an explicit correspondence between segmentation regions and regions enclosed by evolving curves. The algorithm was illustrated on both synthetic and real SAR images. The proposed technique can be improved by introducing a way to estimate the number of regions and can be extended to other representations of SAR images such as vector valued polarimetric SAR images. We are currently addressing both improvements.

Acknowledgments

The authors are grateful to C. Vázquez for letting them use his level-set implementation programs. This work was supported by the Natural Sciences and Engineering Research Council of Canada under strategic grant OGP0004234.

References

[1] T.L. Toan, F. Ribbles, L.F. Wang, N. Floury, K.H. Ding, J.A. Kong, M. Fujita, and T. Kurosu, "Rice Crop Mapping and Monitoring Using ERS-1 Data Based on Experiment and Modeling Results," *IEEE Trans. Geoscience Remote Sensing*, vol. 35, no. 1, pp. 41-55, Jan. 1997.

[2] F. Tupin, H. Maître, J.F. Mangin, J.M. Nicolas, and E. Peshersky, "Detection of Linear Structures in SAR Images: Application to Road Network Extraction," *IEEE Trans. Geoscience Remote Sensing*, vol. 36, no. 2, pp. 434-435, Mar. 1998.

[3] P. Moreels and S.E. Smrekar, "Watershed Identification of Polygonal Patterns in Noisy Sar Images," *IEEE Trans. Image Processing*, vol. 12, no. 7, pp. 740-750, July 2003.

[4] C.J. Oliver, I. McConnell, and R.G. White, "Optimum Edge Detection in SAR," *Proc. SPIE Conf. Satellite Remote Sensing*, pp. 152-163, 1995.

[5] R. Fjørtoft, A. Lopés, P. Marthon, and E. Cubero-Castan, "An Optimum Multiedge Detector for SAR Image Segmentation," *IEEE Trans. Geoscience Remote Sensing*, vol. 36, no. 3, pp. 793-802, 1998.

[6] A.C. Bovik, "On Detecting Edge in Speckle Imagery," *IEEE Trans. Acoustic Speech and Signal Processing*, vol. 36, no. 10, pp. 1618-1627, Oct. 1988.

[7] R. Tousi, A. Lopés, and P. Bousquet, "A Statistical and Geometrical Edge Detector for SAR Images," *IEEE Trans. Geoscience and Remote Sensing*, vol. 26, no. 6, pp. 764-737, Nov. 1988.

[8] O. Germain and P. Réfrégier, "On the Bias of the Likelihood Ratio Edge Detector for SAR Images," *IEEE Trans. Geoscience and Remote Sensing*, vol. 38, no. 3, pp. 1455-1457, May 2000.

[9] L. Vincent and P. Soille, "Watersheds in Digital Spaces: An Efficient Algorithm Based on Immersion Simulations," *IEEE Trans. Pattern Analysis and Machine Intelligence,* vol. 13, no. 6, pp. 583-598, June 1991.
[10] D.M. Smith, "Speckle Reduction and Segmentation of Synthetic Aperture Radar Images," *Int'l J. Remote Sensing,* vol. 17, no. 11, pp. 2043-2057, 1996.
[11] R.F. White, "Change Detection in SAR Imagery," *Int'l J. Remote Sensing,* vol. 12, no. 2, pp. 339-360, 1991.
[12] V.S. Frost, K.S. Shanmugan, and J.C. Holtzman, "A Model for Radar Images and Its Application to Adaptative Filtering of Multiplicative Noise," *IEEE Trans. Pattern Analysis and Machine Intelligence,* vol. 4, no. 2, pp. 157-166, Mar. 1982.
[13] Z. Belhadj and S. Ben Gebara, "Adaptative Speckle Reduction Using Combined Multiresolution Analysis and Prediction Technique," *Int'l J. Remote Sensing,* vol. 23, no. 11, pp. 2236-2282, 2002.
[14] S.C. Zhu and A. Yuille, "Region Competition: Unifying Snakes, Region Growing, and Bayes/MDL for Multiband Image Segmentation," *IEEE Trans. Pattern Analysis and Machine Intelligence,* vol. 18, no. 9, pp. 884-900, Sept. 1996.
[15] C. Samson, L. Blanc-Féraud, G. Aubert, and J. Zerubia, "A Variational Model for Image Classification and Restoration," *IEEE Trans. Pattern Analysis and Machine Intelligence,* vol. 22, no. 5, pp. 460-472, May 2000.
[16] T. Chan and L. Vese, "Active Contours without Edges," *IEEE Trans. Image Processing,* vol. 10, no. 2, pp. 266-277, Feb. 2001.
[17] A. Yezzi, A. Tsai, and A. Willsky, "A Fully Global Approach to Image Segmentation via Coupled Curve Evolution Equations," *J. Visual Comm. and Image Representation,* vol. 13, no. 1, pp. 195-216, Mar. 2002.
[18] C. Vazquez, A. Mitiche, and I. Ben Ayed, "Segmentation of Vectorial Images by a Global Curve Evolution Method," *Proc. Reconnaissance de Forme et Intelligence Artificielle,* Jan. 2004.
[19] C. Vazquez, A. Mitiche, and I. Ben Ayed, "Image Segmentation as Regularized Clustering: A Fully Global Curve Evolution Method," *Proc. IEEE Int'l Conf. Image Processing,* pp. 3467-3470, Oct. 2004.
[20] A.-R. Mansouri, A. Mitiche, and C. Vazquez, "Image Segmentation by Multiregion Competition," *Proc. Reconnaissance de Forme et Intelligence Artificielle,* Jan. 2004.
[21] A.-R. Mansouri, A. Mitiche, and C. Vazquez, "Image Partitioning by Level Set Multiregion Competition," *Proc. IEEE Int'l Conf. Image Processing,* pp. 2721-2724, Oct. 2004.
[22] M. Rousson and R. Deriche, "A Variational Framework for Active and Adaptative Segmentation of Vector Valued Images," *Proc. IEEE Workshop Motion and Video Computing,* pp. 56-61, Dec. 2002.
[23] N. Paragios, O. Mellina-Gottardo, and V. Ramesh, "Gradient Vector Flow Fast Geometric Active Contours," *IEEE Trans. Pattern Analysis and Machine Intelligence,* vol. 26, no. 3, pp. 402-407, Mar. 2004.
[24] C. Samson, L. Blanc-Féraud, G. Aubert, and J. Zerubia, "A Level Set Model for Image Classification," *Int'l J. Computer Vision,* vol. 40, no. 3, pp. 187-197, Mar. 2000.
[25] M. Kass, A. Withkin, and D. Terzopoulos, "Snakes: Actives Contours Model," *Int'l J. Computer Vision,* vol. 1, no. 1, pp. 321-333, Mar. 1988.
[26] O. Germain and P. Réfrégier, "Edge Location in SAR Images: Performance of the Likehood Ratio Filter and Accuracy Improvement with an Active Contour Approach," *IEEE Trans. Image Processing,* vol. 10, no. 4, pp. 72-77, Jan. 2001.
[27] C. Chesnaud, P. Réfrégier, and V. Boulet, "Statistical Region Snake-Based Segmentation Adapted to Different Physical Noise Models," *IEEE Trans. Pattern Analysis and Machine Intelligence,* vol. 21, no. 11, pp. 1145-1157, Nov. 1999.
[28] O. Germain and P. Réfrégier, "Statistical Active Grid for Segmentation Rafinement," *Pattern Recognition Letters,* vol. 22, no. 3, pp. 1125-1132, 2001.
[29] F. Galland, N. Bertaux, and P. Réfrégier, "Minimum Description Length Synthetic Aperture Radar Image Segmentation," *IEEE Trans. Image Processing,* vol. 12, no. 9 pp. 995-1006, Sept. 2003.
[30] J.A. Sethian, *Level Set Methods and Fast Marching Methods,* second ed. Cambridge Univ. Press, 1999.
[31] J.W. Goodman, *Statistical Properties of Laser Speckle Patterns,* Chapter on Laser Speckle and Related Phenomena, pp. 9-75, Springer-Verlag, 1975.
[32] R. Malladi, J.A. Sethian, and B.C. Vemuri, "Shape Modeling with Front Propagation: A Level Set Approach," *IEEE Trans. Pattern Analysis and Machine Intelligence,* vol. 17, no. 2, pp. 158-175, Feb. 1995.

Ismail Ben Ayed received the Bachelor and the Master of Science degrees in telecommunications from the Ecole Superieure des Communications de Tunis (SUP'COM), Tunisie, in 2002 and 2003, respectively. He is currently pursuing the PhD degree at The Institut National de la Recherche Scientifique, center Energie, Materiaux et Telecommunications (INRS-EMT). His research interests include computer vision, level set techniques, and remote sensing. He is a student member of the IEEE.

Amar Mitiche holds a Licence Ès Sciences in mathematics from the University of Algiers and the PhD degree in computer science from the University of Texas at Austin. He is currently a professor in the Telecommunications Department, Institut National de Recherche Scientifique (INRS), Montreal, Quebec, Canada. His research is in computer vision. His current interests include image segmentation, motion analysis in monocular and stereoscopic image sequences (detection, estimation, segmentation, tracking) with a focus on methods based on level set PDEs, and written text recognition with a focus on neural networks methods. He is a member of the IEEE and the IEEE Computer Society.

Ziad Belhadj received the Habilitation universitaire degree in information technology and communication in 2001 and the PhD degree in computer systems from the Ecole Polytechnique de Nantes (Former IRESTE), France, in 1995. After a post-doctoral research position at the Jet Propulsion Laboratory (JPL), he joined the Ecole Superieure des Communictions de Tunis (SUP'COM) in 1996, where he is now a professor, responsible for the Urisa research laboratory and PhD degrees in information technology. His research interests include satellite image processing, speckle denoising from SAR images, remote sensing, image classification, 3D reconstruction, and satellite image indexation. He has (co)authored more than 120 publications in refereed journals and conferences. He is a member of the IEEE.